Optical and Mechanical Properties of Ion-Beam-Sputtered MgF_2 Thin Films for Gravitational-Wave Interferometers

M. Granata,[1,*] A. Amato,[2] M. Bischi,[3,4,†] M. Bazzan,[5] G. Cagnoli,[2] M. Canepa,[6,7] M. Chicoine,[8] A. Di Michele,[9] G. Favaro,[5] D. Forest,[1] G. M. Guidi,[3,4] G. Maggioni,[5] F. Martelli,[3,4] M. Menotta,[10] M. Montani,[3,4] F. Piergiovanni,[3,4] and F. Schiettekatte[8]

[1] *Laboratoire des Matériaux Avancés—IP2I, CNRS, Université de Lyon, Université Claude Bernard Lyon 1, Villeurbanne F-69622, France*

[2] *Université de Lyon, Université Claude Bernard Lyon 1, CNRS, Institut Lumière Matière, Villeurbanne F-69622, France*

[3] *Dipartimento di Scienze Pure e Applicate, Università degli Studi di Urbino Carlo Bo, Urbino I-61029, Italy*

[4] *INFN, Sezione di Firenze, Sesto Fiorentino, Firenze I-50019, Italy*

[5] *Dipartimento di Fisica e Astronomia, Universitá degli Studi di Padova, I-35131, Padova, Italy*

[6] *OPTMATLAB, Dipartimento di Fisica, Università di Genova, Via Dodecaneso 33, Genova 16146, Italy*

[7] *INFN, Sezione di Genova, Via Dodecaneso 33, Genova 16146, Italy*

[8] *Université de Montréal, Montréal, Québec, Canada*

[9] *Dipartimento di Fisica e Geologia, Università degli Studi di Perugia, Via Pascoli, Perugia 06123, Italy*

[10] *Dipartimento di Scienze Biomolecolari, Università degli Studi di Urbino Carlo Bo, Urbino I-61029, Italy*

(Received 25 November 2021; revised 26 January 2022; accepted 2 February 2022; published 23 March 2022)

Brownian thermal noise associated with highly reflective coatings is a fundamental limit for several precision experiments, including gravitational-wave detectors. Research is currently ongoing to find coatings with low thermal noise that also fulfill strict optical requirements such as low absorption and scatter. We report on the optical and mechanical properties of ion-beam-sputtered magnesium fluoride thin films and we discuss the application of such coatings in current and future gravitational-wave detectors.

DOI: 10.1103/PhysRevApplied.17.034058

I. INTRODUCTION

Brownian thermal noise in highly reflective coatings [1,2] is a fundamental limitation for precision experiments such as interferometric gravitational-wave detectors [3], optomechanical resonators [4], and frequency standards [5]. As measured with a laser beam, its power spectral density can be written as [6]

$$S \propto \frac{k_B T}{2\pi f} \frac{d}{w^2} \varphi_c, \tag{1}$$

where k_B is the Boltzmann constant, f is the frequency, T is the temperature, d is the coating thickness, w is the laser-beam radius at which the intensity drops by $1/e^2$, and φ_c is the coating loss angle. The latter quantifies the dissipation of mechanical energy in the coating and is in turn a function of frequency and temperature, $\varphi_c(f, T)$. Thermally induced fluctuations of coated surfaces can thus be reduced by increasing the beam radius, by decreasing the temperature, or by choosing coating materials that minimize the $d\varphi_c$ term in Eq. (1).

High-reflection coatings are usually Bragg reflectors of alternating layers of high and low refractive indices n_H and n_L, respectively. For the same coating transmissivity, the thickness of the layers and the number of layer pairs are a monotonically decreasing function of the refractive index contrast $C = n_H/n_L$. Thus, the higher the contrast C, the lower is the high-reflection coating thickness d and hence the coating thermal noise.

The high-reflection coatings of the Advanced LIGO [7], Advanced Virgo [8], and KAGRA [9] gravitational-wave detectors are thickness-optimized stacks [10] of ion-beam-sputtered (IBS) layers of tantalum pentoxide (Ta_2O_5, also known as *tantala*, high index) and silicon dioxide (SiO_2, *silica*, low index), produced by the Laboratoire des Matériaux Avancés (LMA) [11,12]. Following a procedure developed by the LMA to reduce their optical absorption and loss angle [13], the high-index layers of Advanced LIGO and Advanced Virgo also contain a significant amount of titanium dioxide (TiO_2, *titania*) [14]. Despite the superb optical and mechanical properties of their

*m.granata@lma.in2p3.fr
†matteobischi92@gmail.com

current coatings [12,14,15], coating thermal noise remains a severe limitation for further sensitivity improvement in current gravitational-wave detectors. Thus, in the past two decades, a considerable research effort has been committed to finding alternative coating materials featuring extremely low mechanical and optical losses (absorption, scatter) at the same time [16,17].

The motivation to find alternative coating materials is even stronger for cryogenic gravitational-wave detectors, either present or future, such as KAGRA, the Einstein Telescope [18,19], and Cosmic Explorer [20]. Although, to date, the low-temperature behavior of the loss angles of tantala and titania-tantala coatings is still matter of debate [21–24], the coating loss angle of silica has been conclusively shown to considerably increase below 30 K [25,26].

Because of their low refractive index [27–39], fluoride coatings represent an interesting option for decreasing the thickness and hence the thermal noise of the high-reflection coatings of gravitational-wave detectors. Furthermore, because of their potentially low mechanical loss at low temperature [40], fluorides could be a valid option especially for use at cryogenic temperatures. So far, however, fluoride coatings have never been considered for implementation in gravitational-wave detectors, so that a specifically oriented characterization of their properties is needed.

As a first step toward the development of coatings with low losses, in this paper we report on the optical and mechanical properties of IBS magnesium fluoride (MgF_2) thin films measured at ambient temperature and we discuss their use in gravitational-wave detectors in place of their current low-index silica layers. As postdeposition annealing is a standard procedure to decrease the coating loss angle and the optical absorption, we take special care to characterize its effect on the coating properties.

II. METHODS

A. Samples

Approximately 200-nm-thick layers of IBS MgF_2 are deposited on different substrates: (i) silicon wafers (∅ 75 mm, $t = 0.5$ mm) for optical characterization, ion-beam analysis, and x-ray diffraction measurements; and (ii) fused-silica disks (∅ 50 mm, $t = 1$ mm) for mechanical characterization. Prior to deposition, the fused-silica disks are annealed in air at 900°C for 10 h to release their internal stress due to manufacturing and minimize their intrinsic loss angle φ_0 [41].

The coatings are deposited by the Laser Zentrum Hannover [42] via IBS. Prior to deposition, the base pressure inside the coater vacuum chamber is 5×10^{-6} mbar. The total pressure during the coating process is 2×10^{-4} mbar, with 54 sccm of noble gases (mainly Xe) and gases containing fluorine injected into the chamber. The energy and current of the sputtering ions are 0.9 keV and 0.2 A, respectively, for an average coating deposition rate of 0.1 nm/s. Figure 1 schematically illustrates the layout of the ion-beam source, the sputtering target, and the rotating substrate holder inside the coater vacuum chamber.

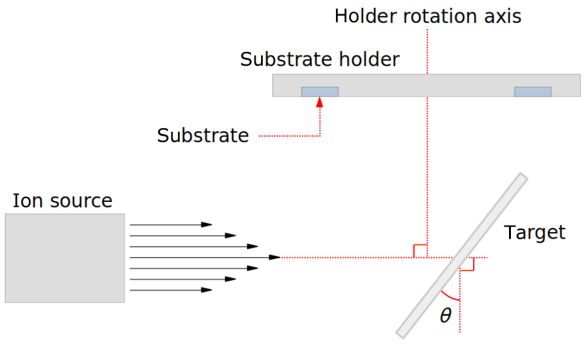

FIG. 1. A schematic view of the IBS system used to produce MgF_2 thin films, where $\theta = 38°$.

All samples are treated together in a first coating run. Then, in order to cancel out the coating-induced curvature that would affect their mode frequencies, the fused-silica disks undergo a second coating run on their other side, under identical conditions.

In order to minimize coating mechanical loss φ_c and optical absorption α, coated samples are thermally treated. The annealing treatments are performed in an Ar atmosphere, at overpressure with respect to the environment, to avoid surface oxidation. We test different soaking temperatures T_a and, with the fused-silica disks only, also different times Δt_a. More specifically, disk A undergoes a series of treatments of increasing soaking temperature, each one of the same duration, while disk B undergoes a series of treatments of increasing time, each one performed at the same soaking temperature. The parameters used for the annealing runs of the fused-silica disks are summarized in Tables I and II.

In between the measurements, all samples are stored under primary vacuum (10^{-2}–10^{-1} mbar) to mitigate oxidation from air exposure.

TABLE I. The soaking temperature T_a and time Δt_a of the annealing treatments applied to fused-silica disk A. Heating and cooling ramps of 100°C/h are used.

	Treatment				
	1	2	3	4	5
T_a (°C)	120	200	285	311	373
Δt_a (h)	10	10	10	10	10

TABLE II. The soaking temperature T_a and time Δt_a of the annealing treatments applied to fused-silica disk B. Heating and cooling ramps of 100°C/h are used.

	Treatment			
	1	2	3	4
T_a (°C)	285	285	285	285
Δt_a (h)	10	20	30	64
Cumulative time (h)	10	30	60	124

B. Structure and chemical composition

In order to determine the microscopic structure of the coating samples, as well as their change upon annealing, we perform a series of grazing-incidence x-ray diffraction (GI-XRD) measurements with a Philips MRD diffractometer, equipped with a Cu tube operated at 40 kV and 40 mA. The probe beam is collimated and partially monochromatized to the Cu $K\alpha$ line by a parabolic multilayer mirror, whereas the detector is equipped with a parallel-plate collimator to define the angular acceptance.

Rutherford backscattering spectrometry (RBS) and elastic recoil detection with time-of-flight detection (ERD TOF) [43] are used to determine the composition of the coating samples, after deposition and after the different annealing steps. RBS measurements are carried out using ^{4}He beams: at 2 MeV in order to rely on the Rutherford cross section of O and F and at 3.7 MeV to better resolve the different elements. The beam is incident at an angle of 7° from the normal and the detector is placed at a scattering angle of 170°. For ERD TOF, a 50-MeV Cu beam is incident at 15° from the sample surface and the TOF camera is at 30° from the beam axis.

C. Optical properties

We use two J. A. Woollam spectroscopic ellipsometers to measure the coating optical properties and thickness, covering complementary spectral regions from the ultraviolet to the infrared: a VASE for the (0.73–6.53)-eV photon-energy range [corresponding to a (190–1700)-nm wavelength range] and a M-2000 for the (0.74–5.06)-eV range (245–1680 nm). The coated Si wafers are measured in reflection and their complex reflectance ratio is characterized by measuring its amplitude component Ψ and phase difference Δ [44]. To maximize the response of the instruments, (Ψ, Δ) spectra are acquired at different incidence angles ($\theta = 50°$, 55°, and 60°) close to the coating Brewster angle. The coating refractive index and thickness are derived by fitting the spectra with realistic optical models [44]. The optical response of the bare Si wafers has been characterized with prior dedicated measurements. Further details about our ellipsometric analysis are available elsewhere [15].

We use photothermal deflection [45] to measure the coating optical absorption at $\lambda = 1064$ nm with an accuracy of less than 1 part per million (ppm).

D. Mechanical properties

Two nominally identical fused-silica disks, labeled A and B, are used for the characterization of the coating mechanical properties. We measure their mass with an analytical balance, before and after each treatment (coating deposition, annealing runs) and their diameter with a caliper. We then use the measured coated area, the coating thickness from ellipsometric measurements, and the mass values to calculate the coating density ρ.

We use the ring-down method [46] to measure the frequency f and ring-down time τ of the first vibrational modes of each fused-silica disk, before and after the coating deposition, and calculate the coating loss angle

$$\varphi_c = \frac{\varphi + (D-1)\varphi_0}{D}, \tag{2}$$

where $\varphi_0 = (\pi f_0 \tau_0)^{-1}$ is the measured loss angle of the bare substrate and $\varphi = (\pi f\, \tau)^{-1}$ is the measured loss angle of the coated disk. D is the frequency-dependent measured *dilution factor* [47],

$$D = 1 - \frac{m_0}{m}\left(\frac{f_0}{f}\right)^2, \tag{3}$$

where m_0 and m are the disk mass as measured before and after the coating deposition, respectively.

We measure modes from approximately 2.5 to approximately 39 kHz for each fused-silica disk, in a frequency band that partially overlaps with the detection band of ground-based gravitational-wave detectors (10–10^4 Hz). In order to avoid systematic damping from suspension and ambient pressure, we use two clamp-free in-vacuum Gentle Nodal Suspension (GeNS) systems [48], shown in Fig. 2. This kind of system is currently the preferred solution of the Virgo and LIGO Collaborations for performing internal friction measurements [14,49].

The fused-silica disks are first measured at the LMA before and after coating deposition and then measured, annealed, and measured again at the Università degli Studi di Urbino Carlo Bo (UniUrb). After deposition, the coating Young's modulus Y and Poisson ratio ν are estimated by fitting finite-element simulations to the measured dilution factor via least-squares numerical regression, where we use values of the substrate thickness previously determined by fitting the measured mode frequencies with a specific subset of simulations [14]. Further details about our GeNS systems, the finite-element simulations, and the data analysis are available elsewhere [14,50].

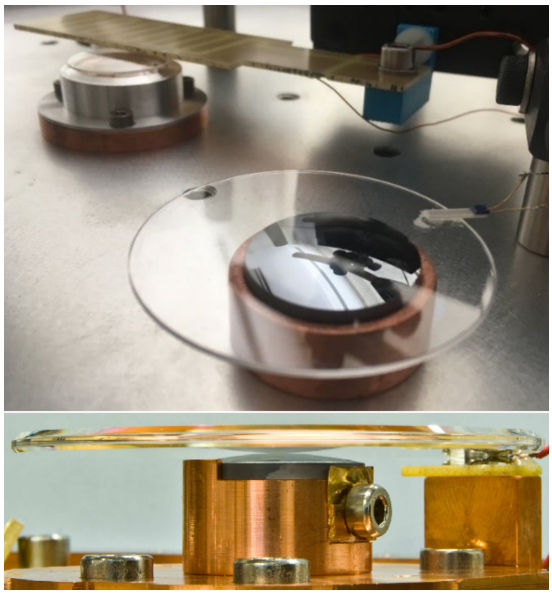

FIG. 2. The GeNS systems used at UniUrb (top) and at the LMA (bottom) to measure the mechanical properties of the thin films.

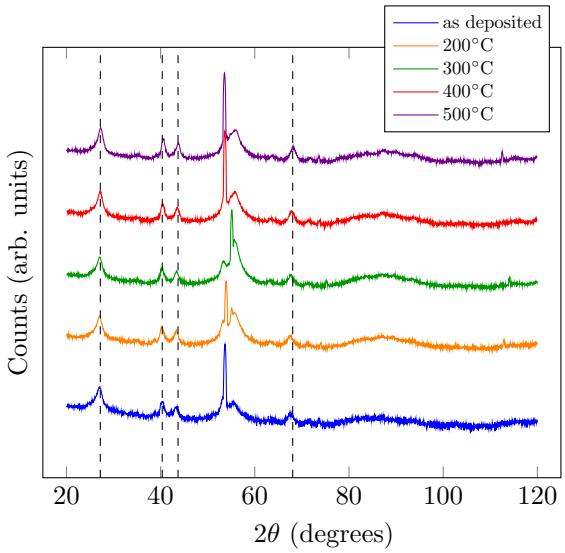

FIG. 3. GI-XRD diffractograms of the IBS MgF_2 thin films on silicon wafers, acquired before and after annealing at different soaking temperatures T_a. The diffraction peaks at about 27°, 40°, 44°, and 68° match fairly well with the 2θ values expected for a crystalline tetragonal structure (JCPDS 70-2269, vertical dashed lines) [32,34,37], while the peaks between 50° and 60° are mainly due to the background signal of the silicon substrate.

III. RESULTS

A. Structure and chemical composition

The GI-XRD diffractograms of the coating samples are shown in Fig. 3, where it can be seen that diffraction peaks at about 27°, 40°, 44°, and 68° are already present in the as-deposited coating. Those peaks fairly match the 2θ values expected for a crystalline tetragonal structure (JCPDS 70-2269) [32,34,37]. Other peaks between 50° and 60° are mainly due to the background signal of the silicon substrate. The change of the coating peaks is minimal for the annealed samples, as they become just slightly higher and narrower. The presence of a polycrystalline phase in the coatings is particularly relevant for gravitational-wave detectors, since it is usually a source of scattered light and hence of optical loss and noise.

The results of the RBS measurements are listed in Table III. The relative atomic concentrations and the density ρ are deduced from SIMNRA simulations [51] of the RBS spectrum acquired on each sample. The Mg:F concentration ratio is compatible with 0.5 for all samples, before and after annealing, within the measurement uncertainty. In addition, all samples contain 3%–5% O and 0.4%–0.5% H and are contaminated by the sputtering gas (0.5%–0.8% Xe) and by Mo from the sputtering source grids. The Mo content increases from about 0.4% at the substrate interface to 0.7% near the surface. All the samples also contain traces of Cu, Ar, and Ta ($< 0.1\%$). The areal atomic density found with RBS can be divided by the layer thickness measured via spectroscopic ellipsometry (206 nm), to find a coating density ρ close to 3.0 g/cm^3 for all samples. According to our analysis, the sample annealed at $T_a = 500$°C also features a 3.7-nm-thick top layer of MgO, assuming an MgO bulk density of 3.85 g/cm^3; hence, this sample apparently suffers from some surface degradation due to oxidation.

B. Optical properties

By way of example, Fig. 4 shows (Ψ, Δ) spectra of the as-deposited coatings, acquired at an incidence angle $\theta = 60°$. As the band gap of crystalline magnesium fluoride is 10.8 eV [52], we initially expect the MgF_2 coatings to be transparent in the energy region probed by our ellipsometers. Instead, preliminary measurements show that some optical absorption in the ultraviolet region has to be taken into account, in order to explain the observed degradation of data quality above 5.7 eV, where the signal-to-noise ratio is drastically reduced, and to correctly fit our data. Such absorption could be explained by the presence of color centers [32,33], as well as by the observed 0.5%–0.7% Mo contamination or the O-related centers due to the 5% O in the samples. We then use a two-pole function and a Tauc-Lorentz oscillator for the optical model of the thin films, which better reproduces the data and simultaneously fits all the measured spectra with the same accuracy. In particular, the pole in the ultraviolet region takes into account absorption at higher photon energies, which affects the real part of the dielectric function in the measurement region, and the pole in the infrared region allows the refractive index to have an inflection point.

TABLE III. The relative atomic concentrations (%) and the density ρ of the IBS MgF_2 thin films, before and after annealing at different soaking temperatures T_a, deduced from SIMNRA simulations [51] of the RBS spectrum acquired on each sample. The Mg:F ratio is in at./at. and the density is calculated by assuming a layer thickness of 206 nm for all samples, as measured via spectroscopic ellipsometry on as-deposited samples.

	Mg	F	O	H	Ar	Cu	Mo[a]	Xe	Ta	Al	Mg:F	ρ (g/cm^3)
As deposited	32.2	63	3	0.4	0.04	0.05	0.53	0.52	0.01	0.6	0.51	2.96 ± 0.05
200°C	31.5	62	5	0.5	0.04	0.05	0.53	0.71	0.01		0.51	2.97 ± 0.05
300°C	31.1	62	5	0.5	0.04	0.05	0.60	0.69	0.01	0.5	0.50	3.00 ± 0.05
400°C	30.8	62	5	0.5	0.08	0.05	0.56	0.60	0.01		0.49	2.98 ± 0.05
500°C[b]	30.4	63	5	0.4	0.04	0.05	0.61	0.84	0.01		0.48	2.83 ± 0.05

[a]The Mo concentration decreases with depth in all samples, from about 0.7% at the surface to about 0.45% at the substrate interface; average values are shown.
[b]The sample annealed at $T_a = 500$°C features an MgO surface layer that is approximately 4 nm thick.

The Tauc-Lorentz model describes the optical absorption but the exact energy of the oscillator cannot be accurately determined, due to the poor data quality in the ultraviolet region. However, for the same reason, the data for $E > 5.7$ eV have a negligible influence on the fit algorithm and the results are compatible with those obtained by fitting the data up to 5.5 eV and extrapolating the values to higher photon energies.

Figure 5 shows the dispersion law and the extinction curve derived from our analysis of the as-deposited coating data and Table IV lists our results against those that we find in the literature concerning IBS MgF_2 thin films [27,31,32,35,36]. The values at $E = 1.17$ eV and $E = 0.80$ eV are particularly relevant, since those photon energies correspond to 1064 and 1550 nm, respectively, which are the operational laser wavelengths of current and future gravitational-wave detectors [7–9,18]. The refractive-index values are $n = 1.405 \pm 0.005$ at 1064 nm and $n = 1.401 \pm 0.005$ at 1550 nm. For comparison, the refractive index at 1064 nm of the IBS silica coatings of present detectors is $n = 1.47 \pm 0.01$ before annealing [14]. Extinction at 6.4 eV (193 nm) is considerably higher than the value reported in the literature [35,36], due to the high absorption that we observe in the ultraviolet region of the spectra.

Figure 6 shows the extinction coefficient k obtained from the photothermal-deflection measurements of optical absorption at 1064 nm, as a function of the annealing temperature T_a. We assume that loss by light scatter is negligible. We obtain $k = 1.1 \times 10^{-4}$ before treatment, which is about 3 orders of magnitude larger than that of the as-deposited silica layers of current gravitational-wave detectors. Although we expect the extinction to be approximately of the same order of magnitude at longer wavelengths, work is currently ongoing to upgrade our apparatus in order to perform sensitive measurements also at 1550 and possibly 2000 nm, which are relevant wavelengths for future detectors [18,20].

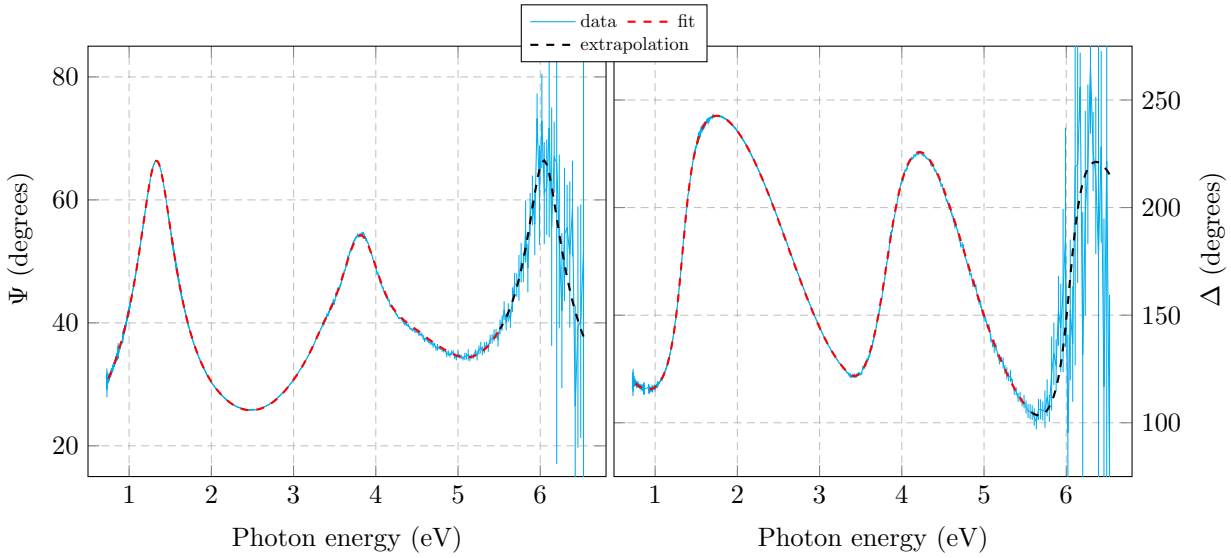

FIG. 4. Measured ellipsometric spectra of the IBS MgF_2 thin films, acquired at an incidence angle $\theta = 60°$.

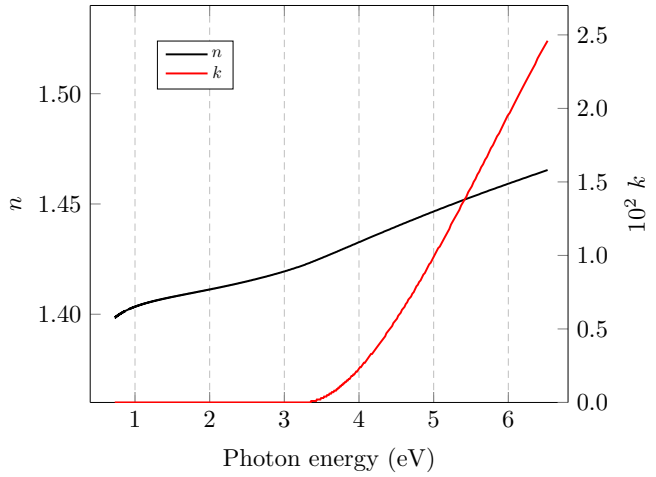

FIG. 5. The refractive index n and extinction coefficient k of the as-deposited IBS MgF_2 thin films as a function of the photon energy, derived from ellipsometric measurements. The relevant values for present and future gravitational-wave detectors are 0.80 and 1.17 eV, corresponding to a laser wavelength of 1550 and 1064 nm, respectively. For energy values smaller than approximately 3.5 eV, the extinction is smaller than the sensitivity of the ellipsometers ($k < 10^{-3}$).

The first annealing step at $T_a = 200°C$ decreases the extinction by 27% but subsequent treatments at higher temperature considerably increase it. Thus, the annealing temperature for minimum extinction due to optical absorption is between 200 and 300°C.

C. Mechanical properties

The main features of fused-silica disks A and B used for the measurements are presented in Table V.

Besides the fact of providing a cross-check of the results, the use of two independent GeNS systems allows us to identify and correct for a systematic effect due to the sample temperature, as described in the following.

By definition, the measured dilution factor D is very sensitive to variations of frequencies and masses. As shown by Fig. 7, $\Delta D/D$ can be as high as approximately 15% if $\Delta f/f$ and $\Delta m/m$ are both of the order of 0.01%. Indeed, the frequency ratio in Eq. (3) depends on the Young's modulus of the sample, which is in turn temperature dependent. For temperatures close to or higher than 300 K and in a limited temperature range, the relative variation of the sample Young's modulus with temperature is a constant [53], $\eta = (dY/dT)/Y$, whereas the sample mode frequencies are proportional to the square root of the Young's modulus, $f \propto \sqrt{Y}$ [54]. Thus we expect that

$$\ln \frac{f(T)}{f(T_0)} = \frac{\eta}{2}(T - T_0), \tag{4}$$

where $f(T)$ is the mode frequency at temperature T. Our GeNS system at the LMA is installed in a cleanroom,

TABLE IV. The refractive index n, extinction coefficient k, and density ρ of the as-deposited IBS MgF_2 thin films. The n and k values presented in this work are measured in the (190–1680)-nm wavelength range via spectroscopic ellipsometry. The k value at 1064 nm is deduced from photothermal-deflection measurements of the optical absorption, by assuming negligible scatter loss.

E (eV)	λ (nm)		This work	Allen *et al.* [27]	Bosch *et al.* [31]	Quesnel *et al.* [32]	Günster *et al.* [35]	Yoshida *et al.* [36]
0.80	1550	n	1.401 ± 0.005		1.380[a]			
		k	$< 10^{-3}$		1.5×10^{-5}[a]			
0.94	1320	n	1.403 ± 0.005		1.380[a]			
		k	$< 10^{-3}$	7×10^{-4}	1.7×10^{-5}[a]			
1.17	1064	n	1.405 ± 0.005		1.380[a]			
		k	$(1.062 \pm 0.004) \times 10^{-4}$	5×10^{-4}	2.0×10^{-5}[a]			
1.96	633	n	1.411 ± 0.005	1.453 ± 0.023	1.383			
		k	$< 10^{-3}$		4.2×10^{-5}			
3.53	351	n	1.426 ± 0.005		1.391	1.390–1.41		
		k	$< 10^{-3}$		1.7×10^{-4}	8×10^{-6}–3.3×10^{-2}		
6.42	193	n	1.46[a]				1.44–1.45	1.44
		k	0.024[a]				$(2–5) \times 10^{-3}$	2×10^{-4}
		ρ (g/cm^3)	2.7 ± 0.2	3.18				

[a]Extrapolations.

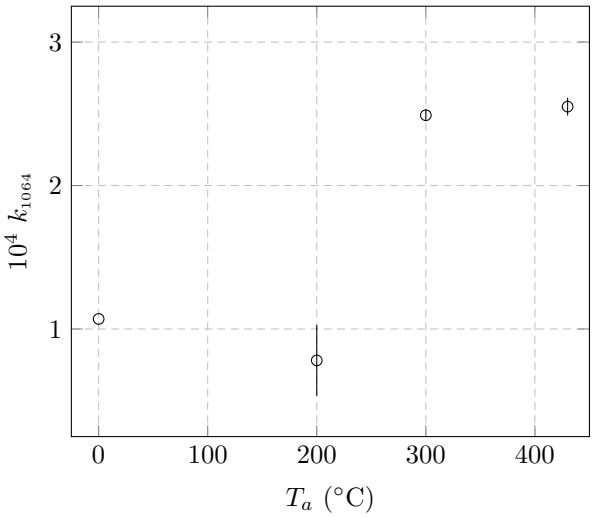

FIG. 6. The extinction coefficient k_{1064} of the IBS MgF_2 thin films as a function of the annealing temperature T_a, obtained from photothermal-deflection measurements of optical absorption performed at 1064 nm ($T_a = 0$°C denotes as-deposited coatings).

where the temperature is stabilized to (21.9 ± 0.5)°C, while our GeNS system at UniUrb is in a room without temperature control. Each setup has a temperature probe in its vacuum tank: right under the GeNS copper base plate at the LMA and on a twin suspended sample [55] at UniUrb (visible in the foreground of Fig. 2). In order to measure the change of resonant frequencies with temperature, we install heating strips around the vacuum tank of the GeNS system at UniUrb and slowly heat a fused-silica bare disk, monitoring the frequency of its first mode. That bare disk is nominally identical to disks A and B, from their same batch. Afterward, we also apply the same procedure to coated disk B. Figure 8 shows the results of those measurements. We obtain $\eta = (1.50 \pm 0.01) \times 10^{-4}\ ^\circ\mathrm{C}^{-1}$ for the bare disk and $\eta = (1.58 \pm 0.01) \times 10^{-4}\ ^\circ\mathrm{C}^{-1}$ for coated disk B, by linearly fitting the data on a semilogarithmic scale. We then use these values to perform a correction

TABLE V. The coated fused-silica disks used to characterize the coating mechanical properties: diameter ∅, substrate thickness d_0, mass m_0 before coating, mass m after coating, and coating thickness d on each side.

	A	B
∅ (mm)	49.77 ± 0.03	49.92 ± 0.01
d_0 (mm)	1.09 ± 0.01	1.08 ± 0.01
m_0 (g)	4.6158 ± 0.0001	4.6348 ± 0.0001
m (g)	4.6180 ± 0.0001	4.6369 ± 0.0004
d (nm)	206 ± 2	206 ± 2

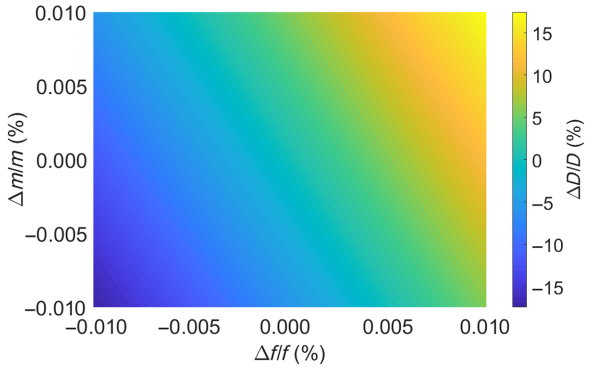

FIG. 7. The relative error $\Delta D/D$ on the dilution factor as a function of the relative errors $\Delta f/f$ and $\Delta m/m$ on the frequency and mass, respectively, for disk B ($f_0 = 2681.062$ Hz, $f = 2682.759$ Hz). For more details, see Eq. (3) and Table V.

of the measured mode frequencies by an amount

$$\Delta f = \frac{\eta}{2}(T - T_0)\, f(T_0) \tag{5}$$

for the data for both fused-silica disks, A and B. This correction is critical whenever mode frequencies are measured in a system where the temperature may drift.

Figure 9 shows the dilution factor and loss angles of fused-silica disks A and B, as measured at the LMA. In the (2.5–39)-kHz frequency band, the mechanical loss of the as-deposited IBS MgF_2 coatings ranges from about 5.5×10^{-4} to 7.5×10^{-4} rad, that is, 20–30 times higher than that of the as-deposited silica layers of current gravitational-wave detectors [14]. This excess loss might be partly explained by the polycrystalline phase of the MgF_2 coatings.

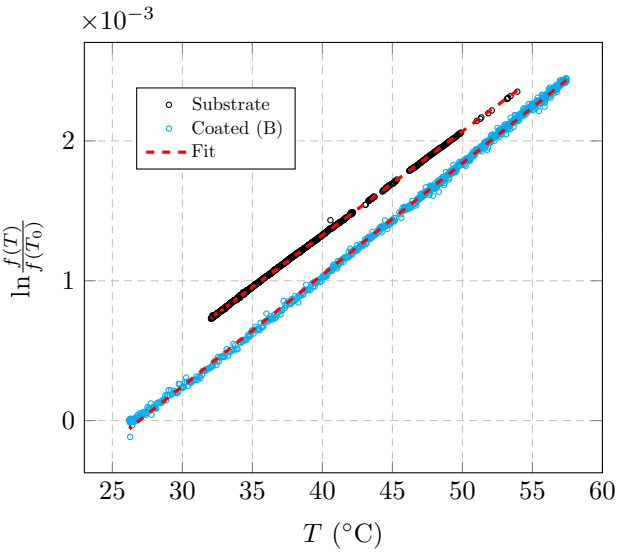

FIG. 8. Variation of the mode frequency $f(T)$ as a function of the sample temperature T, for a fused-silica bare disk and coated disk B.

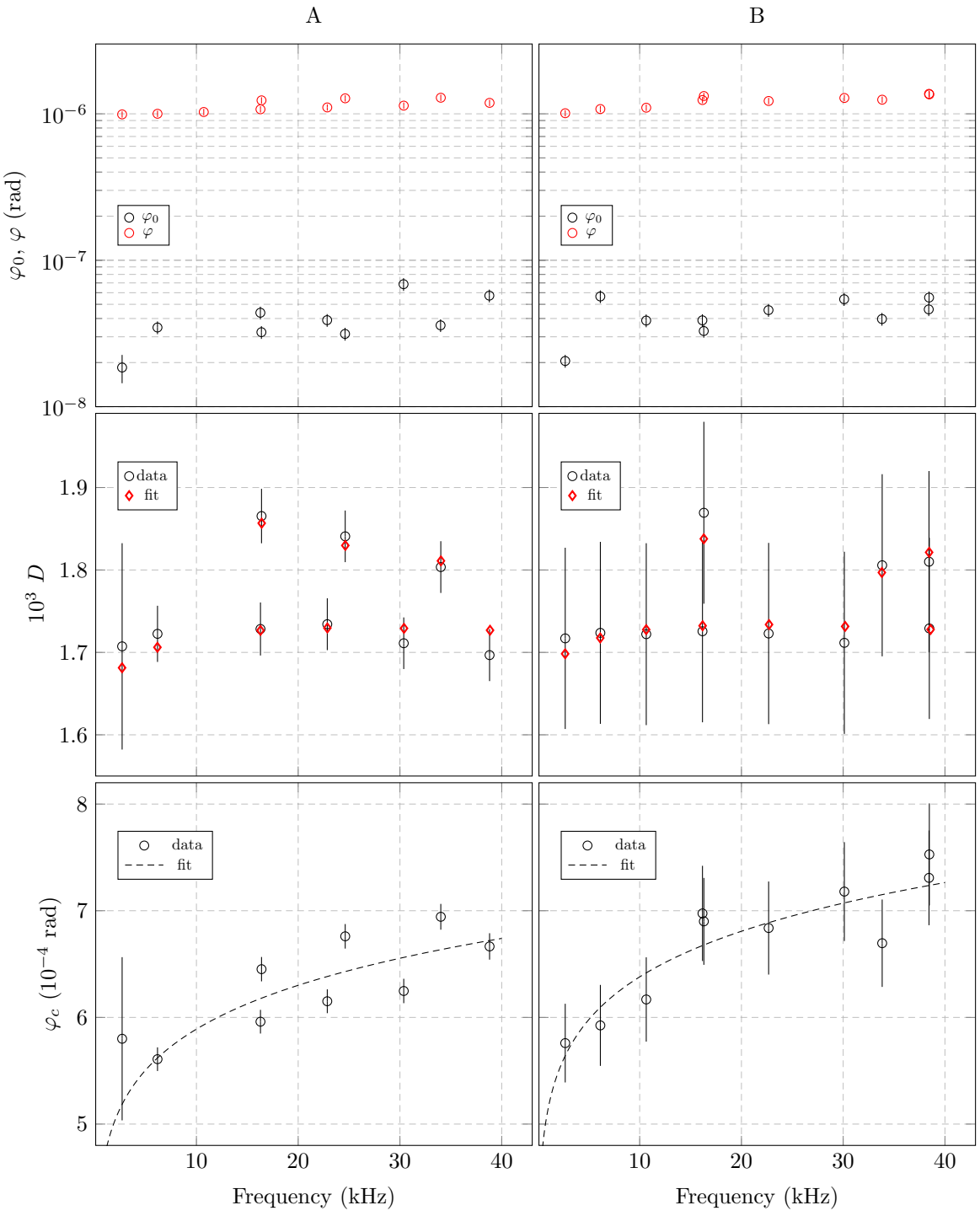

FIG. 9. The characterization of the loss angles of fused-silica disks A (left column) and B (right column), as a function of the frequency. Top row: the measured loss angles before and after deposition of the IBS MgF_2 thin films (φ_0 and φ, respectively). Middle row: a comparison between the measured and least-squares best-fit simulated dilution factors D. Bottom row: the coating loss angle φ_c of the as-deposited IBS MgF_2 thin films; the best-fit power-law model of Eq. (6) is also shown (dashed line). For more details, see Eq. (2).

For comparison, Kinbara *et al.* measured a coating loss angle of 3.5×10^{-4} to 5×10^{-4} rad at 30 Hz on thermally evaporated MgF_2 thin films [56,57]. Such different values could be explained by the different frequency of their measurement and possibly also by the different nature of their thin films, grown with a different technique.

TABLE VI. The measured mechanical properties of the as-deposited IBS MgF_2 thin films: the Young's modulus Y, the Poisson ratio ν, and the best-fit parameters of the power-law model of Eq. (6) used to describe the observed frequency-dependent behavior of the coating loss angle.

	Y (GPa)	ν	a (10^{-4} rad)	b
Disk A	115 ± 3	0.28 ± 0.02	6.4 ± 0.1	0.09 ± 0.02
Disk B	115 ± 3	0.26 ± 0.02	5.9 ± 0.2	0.10 ± 0.03

In order to describe the observed frequency-dependent behavior of the coating loss angle, we fit a power-law model [41,58,59],

$$\varphi_c(f) = a\left(\frac{f}{10\ \text{kHz}}\right)^b, \tag{6}$$

to our data via least-squares linear regression. Table VI lists the best-fit parameters (a, b) for each measured fused-silica disk, together with the best-fit estimations of the coating Young's modulus Y and the Poisson ratio ν obtained via the dilution-factor fitting procedure described in Sec. II D. By taking the average of the results obtained with the two coated disks A and B, we obtain $Y = 115$ GPa and $\nu = 0.27$. Kinbara *et al.* [56,57] obtained $Y = 70$ GPa and $Y = 150$ GPa by applying the resonant method to two different substrates, but could not identify the reason for such a discrepancy. Our results fall within that range.

For the as-deposited samples, we obtain a density ρ of 2.7 ± 0.2 g/cm^3 from the coating mass and thickness ellipsometric measurements, a value fairly close to, but lower than, that of 2.96 g/cm^3 obtained via RBS. Similarly to the coating sample annealed at 500°C, which has the lowest density as measured through RBS ($\rho = 2.83$ g/cm^3), this might be explained by the fact that the samples used for the characterization of the coating mechanical properties suffer from some surface oxidation, despite their storage under primary vacuum.

Figure 10 shows the effect of the postdeposition annealing treatments on the average coating loss angle of disks A and B, calculated from several exemplary modes at different frequencies. For this data, acquired without temperature stabilization at UniUrb, we apply the frequency correction described by Eq. (5). As we increase the annealing temperature up to $T_a = 311$°C, the average coating loss of disk A monotonically decreases from the initial value of $(5.9 \pm 0.7) \times 10^{-4}$ rad to $(2.0 \pm 1.3) \times 10^{-4}$ rad. After treatment at $T_a = 373$°C, however, its average coating loss increases to $(8.4 \pm 3.6) \times 10^{-4}$ rad. Such a substantial increase might be explained by the appearance of cracks on the coating surface, observed on disk A with an optical microscope and shown on Fig. 11, likely due to the fact that the SiO_2 substrate and the MgF_2 coatings have different thermal expansion coefficients. Similar cracks have previously been observed by Kinbara *et al.* and ascribed to the relaxation of accumulated stress [56,57]. Regardless, the annealing temperature for the minimum coating loss angle φ_c is around $T_a = 311$°C.

Concerning the annealing time, in order to avoid the formation of cracks, we use a soaking temperature $T_a = 285$°C for our tests. The average coating loss angle of disk B decreases after each step until the cumulative time of treatment amounts to 30 h, when it is $(3.5 \pm 1.4) \times 10^{-4}$ rad. However, the change in coating loss between the step of 10 h and those of longer cumulative soaking time is negligible, when compared to the measurement uncertainty.

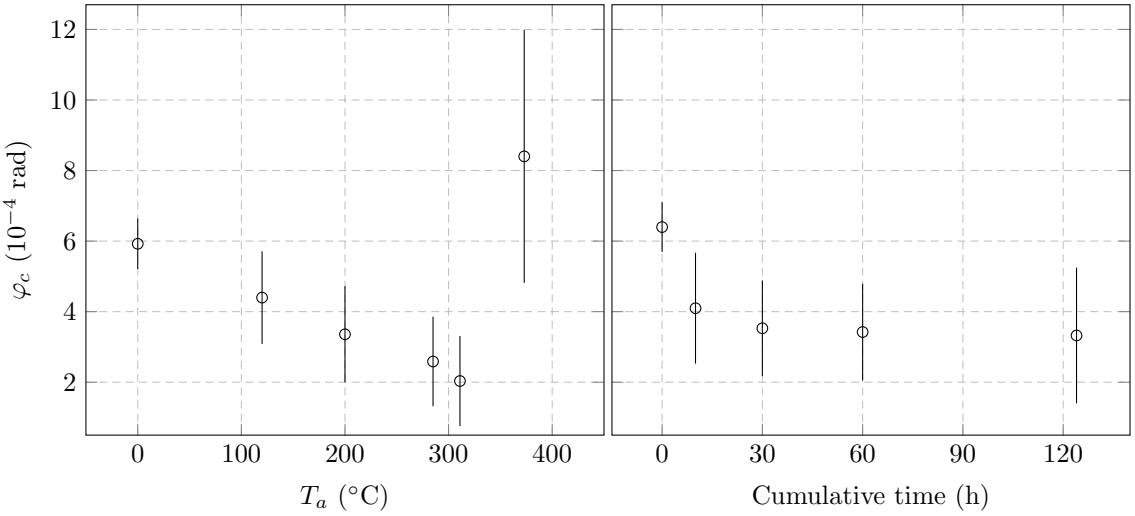

FIG. 10. The coating loss angle φ_c of the IBS MgF_2 thin films, as a function of the annealing temperature T_a for a soaking time $\Delta t_a = 10$ h (left) and of the cumulative soaking time at temperature $T_a = 285$°C (right). For more details, see Tables I and II ($T_a = 0$°C denotes as-deposited coatings).

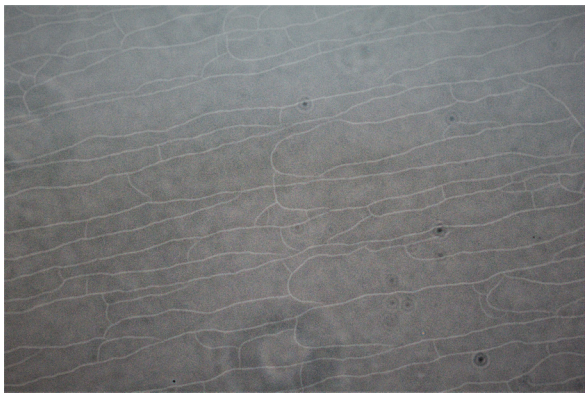

FIG. 11. Cracks at the surface of the IBS MgF_2 thin films on disk A, observed after annealing at $T_a = 373°C$.

Thus, in summary, we find that a soaking time longer than 10 h has no effect on the average value of the coating loss angle, for $T_a = 285°C$.

IV. CONCLUSIONS

In the framework of a research activity devoted to finding low-noise coating materials for present and future gravitational-wave detectors [16], we characterize the optical and mechanical properties of a set of IBS MgF_2 thin films. We choose fluoride coatings because of their low refractive index n_L, with the aim of minimizing the overall high-reflection coating thickness d in Eq. (1). As a reminder, d is a monotonically decreasing function of the refractive index contrast $C = n_H/n_L$. Furthermore, because of their potentially low mechanical loss at low temperature [40], fluorides could be a valid option for use in cryogenic detectors.

Indeed, the IBS MgF_2 thin films feature a 4% lower refractive index than that of the IBS silica layers of current detectors [14], at 1064 nm. However, their optical absorption and ambient-temperature loss angle turn out to be considerably higher, likely because they are partially polycrystalline. In order to minimize such losses, the coating samples are thermally treated with an increasing soaking temperature and time. A soaking temperature of $T_a = 285°C$ avoids the formation of cracks and minimizes the value of the coating loss angle, while the lowest optical absorption occurs after thermal treatment at $T_a = 200°C$. As a consequence, the optimal soaking temperature for our set of samples proves to be between 200 and 300°C, where both the coating optical absorption and average loss angle are close to their minimum values. Soaking times longer than 10 h have a negligible effect on the average value of the coating loss angle.

However, regardless of the effects of annealing, the implementation of IBS MgF_2 thin films in gravitational-wave detectors would require their optical absorption to be reduced drastically, by at least by 3 orders of magnitude. Similarly, their ambient-temperature loss angle also proves to be too large by at least one order of magnitude. A lower optical absorption and loss angle could possibly be achieved by changing the coating growth conditions [14], as well as by reducing the amount of impurities. As shown in Table IV, for instance, Bosch *et al.* and Quesnel *et al.* have demonstrated that IBS MgF_2 thin films of significantly lower extinction and refractive index can be produced [31,32]. The polycrystalline phase of the as-deposited coatings, which is usually the source of scattered light, might in principle also be avoided by using different growth conditions.

The optimization of the growth parameters, together with the measurement of the low-temperature mechanical loss angle and of optical absorption at longer wavelengths, will be the object of future studies.

ACKNOWLEDGMENTS

This work has been promoted by the Laboratoire des Matériaux Avancés and partially supported by the Virgo Coating Research and Development (VCR&D) Collaboration. The work carried out at the Université de Montréal is supported by the Fonds de Recherche du Québec - Nature et Technologie through the Regroupement Québecois sur les Matériaux de Pointe, on equipment obtained in part thanks to the Canada Foundation for Innovation and the Natural Sciences and Engineering Research Council (NSERC). We would like to thank M. Gauch, F. Carstens, and H. Ehlers of the Laser Zentrum Hannover for the production of the MgF_2 thin films and for fruitful discussions, as well as M. Fazio for the first and accurate review of the manuscript. In the online document repositories of the LIGO and the Virgo Scientific Collaborations, this work has been assigned document numbers LIGO-P2100113 and VIR-0314D-21, respectively.

[1] P. R. Saulson, Thermal noise in mechanical experiments, Phys. Rev. D **42**, 2437 (1990).
[2] Y. Levin, Internal thermal noise in the LIGO test masses: A direct approach, Phys. Rev. D **57**, 659 (1998).
[3] R. X. Adhikari, Gravitational radiation detection with laser interferometry, Rev. Mod. Phys. **86**, 121 (2014).
[4] M. Aspelmeyer, T. J. Kippenberg, and F. Marquardt, Cavity optomechanics, Rev. Mod. Phys. **86**, 1391 (2014).
[5] D. G. Matei, T. Legero, S. Häfner, C. Grebing, R. Weyrich, W. Zhang, L. Sonderhouse, J. M. Robinson, J. Ye, F. Riehle, and U. Sterr, 1.5μm Lasers with Sub-10 mHz Linewidth, Phys. Rev. Lett. **118**, 263202 (2017).
[6] G. M. Harry, A. M. Gretarsson, P. R. Saulson, S. E. Kittelberger, S. D. Penn, W. J. Startin, S. Rowan, M. M. Fejer, D. R. M. Crooks, G. Cagnoli, J. Hough, and N. Nakagawa,

Thermal noise in interferometric gravitational wave detectors due to dielectric optical coatings, Class. Quantum Grav. **19**, 897 (2002).

[7] J. Aasi *et al.*, (The LIGO Scientific Collaboration), Advanced LIGO, Class. Quantum Grav. **32**, 074001 (2015).

[8] F. Acernese *et al.*, (The Virgo Collaboration), Advanced Virgo: A second-generation interferometric gravitational wave detector, Class. Quantum Grav. **32**, 024001 (2015).

[9] Y. Aso, Y. Michimura, K. Somiya, M. Ando, O. Miyakawa, T. Sekiguchi, D. Tatsumi, and H. Yamamoto, (The KAGRA Collaboration), Interferometer design of the KAGRA gravitational wave detector, Phys. Rev. D **88**, 043007 (2013).

[10] A. E. Villar, E. D. Black, R. DeSalvo, K. G. Libbrecht, C. Michel, N. Morgado, L. Pinard, I. M. Pinto, V. Pierro, V. Galdi, M. Principe, and I. Taurasi, Measurement of thermal noise in multilayer coatings with optimized layer thickness, Phys. Rev. D **81**, 122001 (2010).

[11] L. Pinard, C. Michel, B. Sassolas, L. Balzarini, J. Degallaix, V. Dolique, R. Flaminio, D. Forest, M. Granata, B. Lagrange, N. Straniero, J. Teillon, and G. Cagnoli, Mirrors used in the LIGO interferometers for first detection of gravitational waves, Appl. Opt. **56**, C11 (2017).

[12] J. Degallaix, C. Michel, B. Sassolas, A. Allocca, G. Cagnoli, L. Balzarini, V. Dolique, R. Flaminio, D. Forest, M. Granata, B. Lagrange, N. Straniero, J. Teillon, and L. Pinard, Large and extremely low loss: The unique challenges of gravitational wave mirrors, J. Opt. Soc. Am. A **36**, C85 (2019).

[13] G. M. Harry *et al.*, Titania-doped tantala/silica coatings for gravitational-wave detection, Class. Quantum Grav. **24**, 405 (2007).

[14] M. Granata, A. Amato, L. Balzarini, M. Canepa, J. Degallaix, D. Forest, V. Dolique, L. Mereni, C. Michel, L. Pinard, B. Sassolas, J. Teillon, and G. Cagnoli, Amorphous optical coatings of present gravitational-wave interferometers, Class. Quantum Grav. **37**, 095004 (2020).

[15] A. Amato, S. Terreni, V. Dolique, D. Forest, G. Gemme, M. Granata, L. Mereni, C. Michel, L. Pinard, B. Sassolas, J. Teillon, G. Cagnoli, and M. Canepa, Optical properties of high-quality oxide coating materials used in gravitational-wave advanced detectors, J. Phys. Mater. **2**, 035004 (2019).

[16] M. Granata, A. Amato, G. Cagnoli, M. Coulon, J. Degallaix, D. Forest, L. Mereni, C. Michel, L. Pinard, B. Sassolas, and J. Teillon, Progress in the measurement and reduction of thermal noise in optical coatings for gravitational-wave detectors, Appl. Opt. **59**, A229 (2020).

[17] G. Vajente, L. Yang, A. Davenport, M. Fazio, A. Ananyeva, L. Zhang, G. Billingsley, K. Prasai, A. Markosyan, R. Bassiri, M. M. Fejer, M. Chicoine, F. Schiettekatte, and C. S. Menoni, Low Mechanical Loss TiO_2:GeO_2 Coatings for Reduced Thermal Noise in Gravitational Wave Interferometers, Phys. Rev. Lett. **127**, 071101 (2021).

[18] S. Hild, M. Abernathy, F. Acernese, P. Amaro-Seoane, N. Andersson, K. Arun, F. Barone, B. Barr, M. Barsuglia, and M. Beker *et al.*, Sensitivity studies for third-generation gravitational wave observatories, *Class. Quantum Grav.* **28**, 094013 (2011).

[19] M. Abernathy, *et al. (The ET Science Team)*, *Einstein Telescope conceptual design study*, ET technical note ET-0106C-10, (2011).

[20] B. P. Abbott *et al.*, (The LIGO Scientific Collaboration), Exploring the sensitivity of next generation gravitational wave detectors, Class. Quantum Grav. **34**, 044001 (2017).

[21] I. W. Martin, E. Chalkley, R. Nawrodt, H. Armandula, R. Bassiri, C. Comtet, M.M. Fejer, A. Gretarsson, G. Harry, D. Heinert *et al.*, Comparison of the temperature dependence of the mechanical dissipation in thin films of Ta_2O_5 and Ta_2O_5 doped with TiO_2, Class. Quantum Grav. **26**, 155012 (2009).

[22] I. W. Martin, R. Bassiri, R. Nawrodt, M. M. Fejer, A. Gretarsson, E. Gustafson, G. Harry, J. Hough, I. MacLaren, S. Penn, S. Reid, R. Route, S. Rowan, C. Schwarz, P. Seidel, J. Scott, and A. L. Woodcraft, Effect of heat treatment on mechanical dissipation in Ta_2O_5 coatings, Class. Quantum Grav. **27**, 225020 (2010).

[23] M. Granata, K. Craig, G. Cagnoli, C. Carcy, W. Cunningham, J. Degallaix, R. Flaminio, D. Forest, M. Hart, J.-S. Hennig, J. Hough, I. MacLaren, I. W. Martin, C. Michel, N. Morgado, S. Otmani, L. Pinard, and S. Rowan, Cryogenic measurements of mechanical loss of high-reflectivity coating and estimation of thermal noise, Opt. Lett. **38**, 5268 (2013).

[24] E. Hirose, G. Billingsley, L. Zhang, H. Yamamoto, L. Pinard, C. Michel, D. Forest, B. Reichman, and M. Gross, Characterization of Core Optics in Gravitational-Wave Detectors: Case Study of KAGRA Sapphire Mirrors, Phys. Rev. Appl. **14**, 014021 (2020).

[25] I. W. Martin, R. Nawrodt, K. Craig, C. Schwarz, R. Bassiri, G. Harry, J. Hough, S. Penn, S. Reid, R. Robie, and S. Rowan, Low temperature mechanical dissipation of an ion-beam sputtered silica film, Class. Quantum Grav. **31**, 035019 (2014).

[26] M. Granata, L. Balzarini, J. Degallaix, V. Dolique, R. Flaminio, D. Forest, D. Hofman, C. Michel, R. Pedurand, L. Pinard, B. Sassolas, N. Straniero, J. Teillon, and G. Cagnoli, Internal friction and Young's modulus measurements on SiO_2 and Ta_2O_5 films done with an ultra-high Q silicon-wafer suspension, Arch. Metall. Mater. **60**, 365 (2015).

[27] T. H. Allen, J. P. Lehan, and L. C. McIntyre Jr., in *Optical Thin Films III: New Developments* (SPIE, Bellingham, 1990), Vol. 1323, p. 277.

[28] M. Zukic, D. G. Torr, J. F. Spann, and M. R. Torr, Vacuum ultraviolet thin films. 1: Optical constants of BaF_2, CaF_2, LaF_3, MgF_2, Al_2O_3, HfO_2, and SiO_2 thin films, Appl. Opt. **29**, 4284 (1990).

[29] J. Kolbe, H. Kessler, T. Hofmann, F. Meyer, H. Schink, and D. Ristau, in *Laser-Induced Damage in Optical Materials: 1991, Proc. SPIE* (SPIE, Bellingham, 1990), Vol. 1624, p. 221.

[30] J. Kolbe and H. Schink, in *Thin Films for Optical Systems, Proc. SPIE* (SPIE, Bellingham, 1993), Vol. 1782, p. 435.

[31] S. Bosch, N. Leinfeliner, E. Quesnel, A. Duparré, C. J. Ferré-Borrull, S. Günster, and D. Ristau, in *Optical and Infrared Thin Films, Proc. SPIE* (SPIE, Bellingham, 2000), Vol. 4094, p. 15.

[32] E. Quesnel, L. Dumas, D. Jacob, and F. Peiró, Optical and microstructural properties of MgF_2 UV coatings grown by ion beam sputtering process, J. Vac. Sci. Technol. A **18**, 2869 (2000).

[33] L. Dumas, E. Quesnel, F. Pierre, and F. Bertin, Optical properties of magnesium fluoride thin films produced by argon ion-beam assisted deposition, J. Vac. Sci. Technol. A **20**, 102 (2002).

[34] D. Ristau, S. Günster, S. Bosch, A. Duparré, E. Masetti, J. Ferré-Borrull, G. Kiriakidis, F. Peiró, Etienne Quesnel, and A. Tikhonravov, Ultraviolet optical and microstructural properties of MgF_2 and LaF_3 coatings deposited by ion-beam sputtering and boat and electron-beam evaporation, Appl. Opt. **41**, 3196 (2002).

[35] S. Günster, B. Görtz, D. Ristau, E. Quesnel, G. Ravel, M. Trovó c, and M. Danailov, in *Advances in Optical Thin Films II, Proc. SPIE* (SPIE, Bellingham, 2005), Vol. 5963, p. 156.

[36] T. Yoshida, K. Nishimoto, K. Sekine, and K. Etoh, Fluoride antireflection coatings for deep ultraviolet optics deposited by ion-beam sputtering, Appl. Opt. **45**, 1375 (2006).

[37] H. Yu, H. Qi, Y. Cui, Y. Shen, J. Shao, and Z. Fan, Influence of substrate temperature on properties of MgF_2 coatings, Appl. Surf. Sci. **253**, 6113 (2007).

[38] M. Putkonen, A. Szeghalmi, E. Pippel, and M. Knez, Atomic layer deposition of metal fluorides through oxide chemistry, J. Mater. Chem. **21**, 14461 (2011).

[39] L. V. Rodríguez-de Marcos, J. I. Larruquert, J. A. Méndez, and J. A. Aznárez, Self-consistent optical constants of MgF_2, LaF_3, and CeF_3 films, Opt. Mater. Express **7**, 989 (2017).

[40] C. Schwarz, D. Heinert, P. Seidel, A. Tünnermann, G. Hammond, and R. Nawrodt, Mechanical loss of calcium fluoride at cryogenic temperatures, Phys. Status Solidi A **208**, 2719 (2011).

[41] F. Travasso, P. Amico, L. Bosi, F. Cottone, A. Dari, L. Gammaitoni, H. Vocca, and F. Marchesoni, Low-frequency internal friction in silica glass, EPL **80**, 50008 (2007).

[42] https://www.lzh.de/.

[43] M. Chicoine, F. Schiettekatte, M. I. Laitinen, and T. Sajavaara, Oxy-nitrides characterization with a new ERD-TOF system, Nucl. Instrum. Meth. B **406**, 112 (2017).

[44] H. Fujiwara, *Spectroscopic Ellipsometry: Principles and Applications* (John Wiley & Sons, New York, 2007).

[45] A. C. Boccara, D. Fournier, W. Jackson, and N. M. Amer, Sensitive photothermal deflection technique for measuring absorption in optically thin media, Opt. Lett. **5**, 377 (1980).

[46] A. Nowick and B. Berry, *Anelastic Relaxation in Crystalline Solids* (Academic Press, New York, 1972), p. 582.

[47] T. Li, F. A. Aguilar Sandoval, M. Geitner, L. Bellon, G. Cagnoli, J. Degallaix, V. Dolique, R. Flaminio, D. Forest, M. Granata, C. Michel, N. Morgado, and L. Pinard, Measurements of mechanical thermal noise and energy dissipation in optical dielectric coatings, Phys. Rev. D **89**, 092004 (2014).

[48] E. Cesarini, M. Lorenzini, E. Campagna, F. Martelli, F. Piergiovanni, F. Vetrano, G. Losurdo, and G. Cagnoli, A "gentle" nodal suspension for measurements of the acoustic attenuation in materials, Rev. Sci. Instrum. **80**, 053904 (2009).

[49] G. Vajente, A. Ananyeva, G. Billingsley, E. Gustafson, A. Heptonstall, E. Sanchez, and C. Torrie, A high throughput instrument to measure mechanical losses in thin film coatings, Rev. Sci. Instrum. **88**, 073901 (2017).

[50] M. Granata, Em. Saracco, N. Morgado, A. Cajgfinger, G. Cagnoli, J. Degallaix, V. Dolique, D. Forest, J. Franc, C. Michel, L. Pinard, and R. Flaminio, Mechanical loss in state-of-the-art amorphous optical coatings, Phys. Rev. D **93**, 012007 (2016).

[51] M. Mayer, in *AIP Conference Proceedings* (AIP, College Park, Maryland, 1999), Vol. 475, p. 541.

[52] K. Babu, C. Lingam, S. Auluck, S. Tewari, and G. Vaitheeswaran, Structural, thermodynamic and optical properties of MgF_2 studied from first-principles theory, J. Solid State Chem. **184**, 343 (2011).

[53] J. B. Wachtman, Jr., W. E. Tefft, D. G. Lam, Jr., and C. S. Apstein, Exponential temperature dependence of Young's modulus for several oxides, Phys. Rev. **122**, 1754 (1961).

[54] M. Amabili, A. Pasqualini, and G. Dalpiaz, Natural frequencies and modes of free-edge circular plates vibrating in vacuum or in contact with liquid, Sound Vib. **188**, 685 (1995).

[55] We find no experimental evidence that the laser of the optical lever used to measure the ring-down amplitude of the main sample induces a temperature variation. Therefore, we assume that the temperature measured on the twin sample is equal to that of the main sample.

[56] A. Kinbara, S. Baba, N. Matuda, and K. Takamisawa, Mechanical properties of and cracks and wrinkles in vacuum-deposited MgF_2, carbon and boron coatings, Thin Solid Films **84**, 205 (1981).

[57] A. Kinbara, S. Baba, N. Matuda, and K. Takamisawa, Mechanical properties and deterioration of MgF_2 thin films, Thin Solid Films **89**, 125 (1982).

[58] K. Gilroy and W. Phillips, An asymmetric double-well potential model for structural relaxation processes in amorphous materials, Philos. Mag. B **43**, 735 (1981).

[59] G. Cagnoli, M. Lorenzini, E. Cesarini, F. Piergiovanni, M. Granata, D. Heinert, F. Martelli, R. Nawrodt, A. Amato, Q. Cassar, J. Dickmann, S. Kroker, D. Lumaca, C. Malhaire, and C. B. Rojas Hurtado, Mode-dependent mechanical losses in disc resonators, Phys. Lett. A **382**, 2165 (2018).